Moving Target Imaging for Synthetic Aperture Radar Via RPCA

1st Sean Thammakhoune
Department of Electrical, Computer and Systems Engineering
Rensselaer Polytechnic Institute
110 8th Street, Troy, NY 12180 USA
thamms@rpi.edu

2nd Bariscan Yonel
Department of Electrical, Computer and Systems Engineering
Rensselaer Polytechnic Institute
110 8th Street, Troy, NY 12180 USA
yonelb@rpi.edu

3rd Eric Mason
United States Naval Research Laboratory
4555 Overlook Ave SW, Washington, DC 20375 USA
eric.mason@nrl.navy.mil

4th Birsen Yazici
Department of Electrical, Computer and Systems Engineering
Rensselaer Polytechnic Institute
110 8th Street, Troy, NY 12180 USA
yazicb@rpi.edu

5th Yonina C. Eldar
Department of Mathematics and Computer Science
Weizmann Institute of Science
Herzl Street 234, Rehovot 7610001, Israel
yonina.eldar@weizmann.ac.il

2021 IEEE Radar Conference (RadarConf21) | 978-1-7281-7609-3/20/$31.00 ©2021 IEEE | DOI: 10.1109/RadarConf2147009.2021.9455293

***Abstract*—Synthetic aperture radar (SAR) imaging of moving targets is a challenging task, as standard techniques have been developed for stationary scenes. Motivated by success of robust principal component analysis (RPCA) in change detection for video processing, we establish a rank-1 and sparse decomposition framework for the SAR problem in the image domain. We construct the *phase-space reflectivity* matrix for single-channel SAR systems reconstructing images at various hypothesized velocities and show that it is the superposition of a rank-1 matrix and a disjoint sparse matrix. This structure allows for additional constraints that reduce the computational complexity when compared to generic RPCA. We compare the performances of two algorithms, proximal gradient descent (PGD) and alternating direction method of multipliers (ADMM), on numerical simulations for the moving target imaging problem.**

***Index Terms*—Synthetic Aperture Radar (SAR), Moving Target, Robust PCA, rank-1, convex**

I. Introduction

Synthetic aperture radar (SAR) is used in many defense and remote sensing applications, as it is capable of providing high resolution images independent of weather conditions [1]–[3]. In SAR, a scene of interest is illuminated by electromagnetic waves that are transmitted by an antenna placed on a moving platform in order to generate a synthetic aperture to provide resolution beyond that of the physical antenna by simulating an antenna length much longer than a physical antenna.

Detection of moving targets pose a challenge in SAR imaging since standard processing techniques have been developed for imaging stationary scenes, and thus remains an important problem in a number of SAR modalities [4]–[14]. Moving targets introduce velocity-dependent range variations, leading to smearing artifacts in the reconstructed images [15]–[17]. In GMTI radar with stationary receivers, clutter can be suppressed by filtering out the zero-Doppler components, as the Doppler shift implies velocity information. However, the addition of a moving radar platform in SAR makes indication more complex; due to the movement of the platform, the Doppler spectrum of moving targets and the stationary scene may overlap.

Space-time processing techniques such as displaced phase center antenna (DPCA), along track interferometry (ATI), and space-time adaptive processing (STAP) are classical approaches to the clutter suppression problem in SAR [18]–[24]. DPCA relies on two receivers traversing the same trajectory, simultaneously imaging the same scene [22]. The received signal is then identical for all stationary clutters and the moving targets can be separated by subtracting the two received signals. Similar to DPCA, ATI uses two displaced antennas to detect ground moving targets, utilizing the formed images instead of received signals [23], [24]. In ATI, the first image is multiplied by the complex conjugate of the second, leading to zero phase for the stationary targets and moving targets can be extracted from the non-zero phase components. While computationally efficient, these methods require specific imaging geometries with multiple antennas, increasing operational costs and acquisition complexity. In STAP, a two-dimensional space-time filter adaptively adjusts maximize the output signal-to-interference-plus-noise ratio (SINR), improving the detection of the moving targets [18], [19]. However, STAP is computationally expensive, requiring the need calculate an inverse covariance matrix, and requires target-free training samples which can be difficult when moving target parameters are often unknown.

Motivated by its success in image processing, robust principal component analysis (RPCA) has been used to address GMTI, which aims to separate a data matrix into a low-rank component and a sparse component. A popular approach to

achieve this property is through using multi-channel SAR, in which an antenna array is used to obtain data through multiple receiver channels [25]–[35]. After accounting for phase differences caused by channel spacing, each channel's observation matrix is stacked into a column of a matrix. Each channel then has similar received data except for the moving target parts, thus forming a low-rank plus sparse matrix. In [25], the separation problem is solved via Go Decomposition, which assumes the rank of the low-rank component and the cardinality of the sparse component as prior knowledge. However, these constraints introduce non-convexity to the problem and global convergence is not guaranteed. Furthermore, the performance of these algorithms are heavily dependent on the choice of cardinality. In order to address these issues, [26] extends this work by first estimating low-rank and sparse components through ATI images. While this approach gives a better initial point, it does not address the issue of non-convexity. In [28], a joint multi-channel sparsity approach of RPCA is introduced by assuming the sparsity pattern between channels remains the same and thereby enhancing signal signature. In [29], RPCA is used to find target-free training samples used for STAP for more accurate clutter suppression.

In [32]–[35], subaperture based approaches are used for imaging. In [32], [34], the high resolution SAR image is split into a number of subaperture images in the azimuth direction to exploit a low-rank sparse decomposition (LRSD) framework for SAR images. A discrete Fourier (DFT) transform is applied to a SAR image containing unfocused moving targets, and is followed by a filtering operation to extract frequency domain subapertures. An inverse DFT of the original image size is then performed on zeropadded subapertures to obtain subaperture images. These images are then stacked column-wise to construct a matrix that fits the LRSD framework and decomposition is achieved via alternating direction method of multipliers.

Similar to these approaches, ours relies on the LRSD framework. In contrast to these works, we consider to formulate our model based on the *phase-space reflectivity function* for monostatic SAR systems [7]–[9], [36], [37]. Motivated by RPCA, we construct a finite dimensional matrix that can be decomposed into a rank-1 stationary component and a sparse component associated with moving targets. Using this rank-1 constraint, we reduce the computation time of generic RPCA, as there is no need for a singular value decomposition associated with the singular value threshold. We show that this matrix is formed by two disjoint, orthogonal subspaces allowing for additional constraints to be made on the moving targets other than sparsity. In addition to separating the stationary and moving targets, our approach both focuses the moving target and estimates velocity parameters without the need of a priori knowledge on motion parameters, nor the number of moving targets in the scene. We use two methods of solving the GMTI problem using proximal gradient descent (PGD) and alternating direction method of multipliers (ADMM).

The rest of the paper is organized as follows: In Section II, we present the SAR received signal model. In Section III, we discuss our framework for separating moving targets from stationary clutter. Section IV presents numerical simulations results, and we conclude our discussion in Section V.

II. Forward Models

We consider a monostatic SAR system in which the transmitter and receiver are collocated. We begin by making the start-stop approximation for moving targets in which the target and the antennas only move between pulses, and are stationary during a pulse. Let $s \in [s_0, s_1]$ denote the slow-time, which indexes each data processing window and $\mathbf{x}$ be a location on the ground where $\mathbf{x} = [\boldsymbol{x}, \psi(\boldsymbol{x})] \in \mathbb{R}^3$, $\boldsymbol{x} \in \mathbb{R}^2$ and $\psi : \mathbb{R}^2 \to \mathbb{R}$ is a known smooth function modeling ground topography. Without loss of generality, we let $\mathbf{x}$ be the position of the targets at the beginning of the synthetic aperture, at time $s_0 = 0$. Assuming the scatterer moves at a constant velocity, we can represent the trajectory of the scatterer as $\mathbf{z}(s) = \mathbf{x} + \mathbf{v}_\mathbf{x} s$, where $\mathbf{v}_\mathbf{x} \in \mathbb{R}^3$ is the velocity of a particular point scatterer located at point $\mathbf{x}$ at time $s_0 = 0$. Since the target is moving on the surface, the velocity $\mathbf{v}_\mathbf{x}$ is of the form $\mathbf{v}_\mathbf{x} = [\boldsymbol{\nu}_{\boldsymbol{x}}, \nabla_{\boldsymbol{x}}\psi(\boldsymbol{x}) \cdot \boldsymbol{\nu}_{\boldsymbol{x}}]$, where $\boldsymbol{\nu}_{\boldsymbol{x}}$ is the 2D-velocity of the target and $\nabla_{\boldsymbol{x}}\psi(\boldsymbol{x})$ is the gradient of the ground topography. We define the phase-space reflectivity function of a target as:

$$q(\boldsymbol{x}, \boldsymbol{\nu}) = \rho(\boldsymbol{x})\delta(\boldsymbol{\nu} - \boldsymbol{\nu}_{\boldsymbol{x}}) \tag{1}$$

$$\approx \rho(\boldsymbol{x})\varphi(\boldsymbol{\nu}, \boldsymbol{\nu}_{\boldsymbol{x}}) \tag{2}$$

where $\varphi(\boldsymbol{\nu}, \boldsymbol{\nu}_{\boldsymbol{x}})$ is a smooth, differentiable function of $\boldsymbol{\nu}$ that approximates the Dirac delta function in the limit. Under Born approximation, the received signal model for monostatic SAR is defined as follows [5], [7], [38]:

$$d(s,t) \;=\; \int \mathrm{e}^{-\mathrm{i}\phi(\omega,s,\boldsymbol{x},\boldsymbol{\nu})} A(\omega, s, \boldsymbol{x}, \boldsymbol{\nu}) q(\boldsymbol{x}, \boldsymbol{\nu}) d\omega d\boldsymbol{x} d\boldsymbol{\nu} \tag{3}$$

where t is the fast-time, $\omega \in \mathbb{R}$ is the temporal frequency, $A(\omega, s, \boldsymbol{x}, \boldsymbol{\nu})$ is a complex amplitude function varying slowly in ω that includes transmitter and receiver antenna beam patterns, the transmitted waveforms, geometrical spreading factors, etc. and $\phi(\omega, s, \boldsymbol{x}, \boldsymbol{\nu})$ is the phase function given by $\phi(\omega, s, \boldsymbol{x}, \nu) = \frac{\omega}{c_0}(R(s, \boldsymbol{x}) + B(s, \boldsymbol{x}, \boldsymbol{\nu}))$ with $R(s, \boldsymbol{x})$ being the total travel distance, $B(s, \boldsymbol{x}, \boldsymbol{\nu})$ being the range-variation due to the movement of the scatterer, and c_0 the speed of light. For a monostatic SAR configuration, $R(s, \boldsymbol{x}) = 2|\gamma(s) - \mathbf{x}|$ and $B(s, \boldsymbol{x}, \boldsymbol{\nu}) = 2\widehat{(\mathbf{x} - \gamma(s))} \cdot \boldsymbol{\nu} s$ where $\gamma(s) \in \mathbb{R}^3$ is the location of the transmitter/receiver pair, and $\widehat{(\mathbf{x} - \gamma(s))}$ denotes the unit vector from the transmitter/receiver to the scatterer.

A. Phase-space reflectivity matrix

We now discretize the underlying scene reflectivity function and represent it in the standard pixel basis such that the image domain is sampled on an N-dimensional grid of $D := \{\boldsymbol{x}_k\}_{k=1}^N$. Furthermore, we discretize the range of velocities using $[\Delta\nu_1, \Delta\nu_2]$ intervals into an M-samples to obtain an $M \times N$ sized matrix $\mathbf{Q}$, a matrix formed by reconstructing an image at each constant hypothesized velocity for the entire scene. If the hypothesized velocity is equal to the true velocity

of the scatterer, the scatterer will be reconstructed in its correct initial position. The reconstructed reflectivity images are then stacked into rows of $\mathbf{Q}$, where each image corresponds to a constant hypothesized velocity, and we refer to $\mathbf{Q}$ as the phase-space reflectivity matrix. Since all stationary targets have the same velocity $\boldsymbol{\nu} = 0$, they appear in the same *row* of $\mathbf{Q}$ corresponding to the index $\boldsymbol{\nu} = 0$. Thus, stationary targets form a rank-1 component in $\mathbf{Q}$, which we denote as $\mathbf{Q}_s$. On the other hand, the remaining terms span a subspace in $\mathbb{C}^M$ of dimension equal to the number of unique velocities V within the scene of interest, which is upper-bounded by the number of moving targets. Thus, we propose a decomposition of the unknown matrix $\mathbf{Q}$ to a rank-1 $\mathbf{Q}_s$ and sparse $\mathbf{Q}_\nu$ as follows:

$$\mathbf{Q} = \mathbf{Q}_s + \mathbf{Q}_\nu. \tag{4}$$

III. Moving Target Imaging Via Rank-1 RPCA

Here, we introduce an updated minimization problem for our rank-1 framework of $\mathbf{Q}$. It is well-known in an optimization setting that the nuclear-norm promotes low-rankedness and the ℓ_1-norm promotes sparsity. Typical RPCA seeks to solve the problem

$$\begin{aligned} \min_{\mathbf{Q}_s, \mathbf{Q}_\nu} \ & \|\mathbf{Q}_s\|_* + \lambda \|\mathbf{Q}_\nu\|_1 \\ \text{s.t} \quad & \mathbf{Q}_s + \mathbf{Q}_\nu = \mathbf{Q}, \end{aligned} \tag{5}$$

where $\|\cdot\|_*$ is the nuclear-norm, the sum of singular values of $\mathbf{Q}_s$, and $\|\cdot\|_1$ is the ℓ_1 norm which equals the sum of magnitudes of $\mathbf{Q}_\nu$. Many numerical algorithms exist to solve the LRSD problem [39]–[41], but it is most popularly solved using proximal methods to arrive to an iterative solution. However, the singular value threshold (SVT), the proximal mapping corresponding to the nuclear-norm, is very computationally expensive due to the calculation of the singular value decomposition. Recall that our constructed $\mathbf{Q}$ matrix is the superposition of a rank-1 $\mathbf{Q}_s$ and an orthogonal $\mathbf{Q}_\nu$. We show that we can impose additional constraints to support the structure of $\mathbf{Q}$ and reduce the per-iteration complexity of RPCA.

We construct our objective function by first denoting the index of zero-velocity as ν_c, and define the constraint C_1 as the set of matrices $\mathbf{X}$ that lie in the space formed by $\mathbf{e}_{\boldsymbol{\nu}_c}\boldsymbol{\rho}^H$. Here, $\mathbf{e}_{\nu_c} \in \mathbb{R}^M$ is the standard basis vector that has the 1 entry at index corresponding to ν_c, 0 else, and $\boldsymbol{\rho} \in \mathbb{R}^N$ is a vector of reflectivity coefficients. While rank-1 constraints are typically non-convex, note that since we always have knowledge of the index corresponding to ν_c, C_1 is actually a convex constraint set. Furthermore, recall that $\mathbf{Q}_s$ and $\mathbf{Q}_\nu$ lie in the span of orthogonal subspaces. We introduce a second convex constraint set $C_1^\perp$ as the set of matrices $\mathbf{X}$ that lie in the orthogonal complement of C_1, defined as $C_1^\perp$. Finally, we seek to solve

$$\begin{aligned} \min_{\mathbf{Q}_s, \mathbf{Q}_\nu \in \mathbb{R}^+} \ & \lambda \|\mathbf{Q}_\nu\|_1 \\ \text{s.t} \quad & \|\mathbf{d} - \mathcal{F}(\mathbf{Q}_s + \mathbf{Q}_\nu)\|_F \leq \delta \\ & \mathbf{Q}_s \in C_1, \ \mathbf{Q}_\nu \in C_1^\perp. \end{aligned} \tag{6}$$

We solve (6) via PGD and ADMM and note that rank-1 constraint renders the nuclear-norm redundant. As the rank-1 constraint can be efficiently implemented by a simple projection, we observe that the complexity of both algorithms is significantly reduced as there is no need to calculate an SVD. After successful decomposition of $\mathbf{Q}$, the moving targets can then be reconstructed by searching the rows of $\mathbf{Q}_\nu$ and reshaping them into 2D matrices.

IV. Numerical Experiments

A. Scene and Imaging Parameters

We use a 100 $\times$ 100m^2 scene with a single stationary target discretized into 31 $\times$ 31 pixels. A monostatic radar signal is synthesized according to (3) with $A = 1$. The antenna traverses a circular trajectory defined as $\gamma(s) = [11 + 11\cos(s), 11 + 11\sin(s), 6.5]$km. The center frequency is 9 GHz with a bandwidth of 622 MHz in accordance to the GOTCHA Volumetric SAR dataset [42]. The slow-time and fast-time are sampled uniformly, obtaining 2048 and 100 samples respectively. We note that the assumptions of the moving targets having a linear trajectory while the antennas traverse a complete circular trajectory may not be valid in practice. However, this configuration is chosen to separate the velocity-estimation effects from potential limited-aperture artifacts.

B. Results

1) Multiple moving point targets and stationary extended target: In this set of simulations, there are three moving point targets located in the upper left, upper right, and lower left quadrant of the scene at time $s = 0$ moving at a velocities of $\boldsymbol{\nu}_1 = [10, -14]$ km/hr, $\boldsymbol{\nu}_2 = [4, -16]$ km/hr and $\boldsymbol{\nu}_3 = [10, 0]$ km/hr respectively. A stationary extended target is located in the lower right quadrant of the scene. Figure 1 shows the ground truth scene with antenna trajectories.

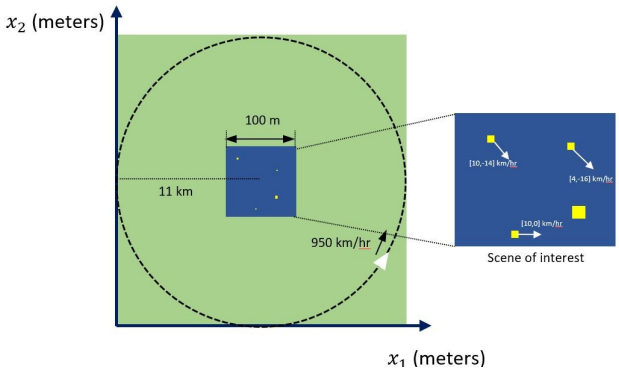

Fig. 1. Illustration of the simulation set-up for a multiple moving targets and a stationary extended target. The dark region shows the scene of interest, where the yellow square shows the position of the target and the white arrows show its velocity components. The antennas traverse a circular flight trajectory, where the white triangle shows the transmitter/receiver pair.

The phase-space reflectivity matrix $\mathbf{Q}$ is constructed using hypothesized velocities ranging from -20 km/hr to 20 km/hr in

both the $x-$ and $y-$directions at $\Delta\nu = 2$ km/hr, resulting in 441 discrete velocities. We perform both PGD and ADMM and consider the ℓ_2-norm error between $\mathbf{Q}$ and $\mathbf{Q}_s + \mathbf{Q}_\nu$. Figure 2 shows a plot of the average error for PGD and ADMM at each iteration. We see that ADMM converges to a solution faster than PGD, but both algorithms arrive to the same solution. Since both algorithms arrive to the same solution, we focus on results from PGD.

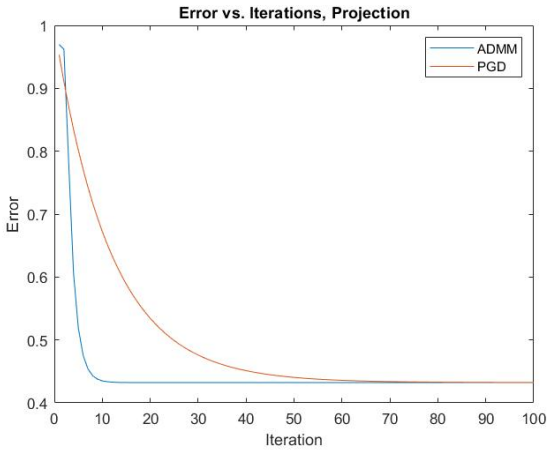

Fig. 2. ℓ_2-norm error vs. iterations for PGD (orange) and ADMM (blue).

For a visual demonstration, we display the reconstructed moving targets. We search the rows of the obtained $\mathbf{Q}_\nu$ to obtain the hypothesized velocities obtained by the algorithms. Figure 3 shows that the algorithm recovers the correct velocities. This results in the reconstructed moving targets being focused in the correct positions; the superposition of each reconstructed moving target at their estimated velocities as well as the reconstruction of the stationary component are shown in Figure 4.

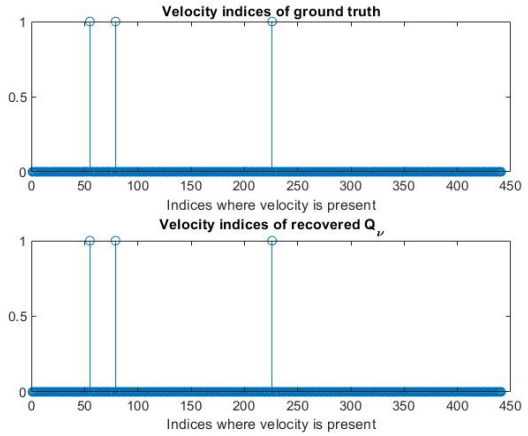

Fig. 3. Indices of moving target velocities for ground truth (top) and reconstruction (bottom).

2) Signal-to-noise ratio: In this set of simulations, we vary the signal-to-noise ratio (SNR) of the received signal data by

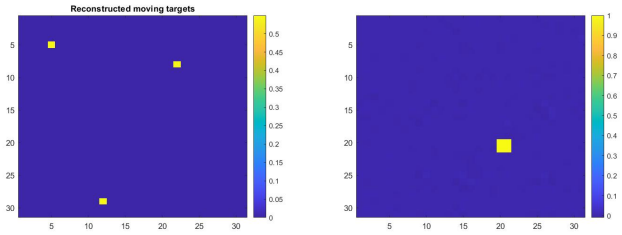

Fig. 4. The reflectivity image reconstructed using the estimated velocities (left) and the reconstruction of the stationary component (right).

adding white Gaussian noise to the signal. We use the same imaging and scene parameters as previous sections. Here, SNR is defined by $10\log(\sigma_d/\sigma_n)$, where σ_d is the standard deviation of the received signal data, and σ_n is the standard deviation of the noise. We varied the SNR of the received signal from -20dB to +20dB with a step-size of +2dB and used structural similarity index (SSIM) between the ground truth moving targets and reconstructed moving targets as a performance metric. Figure 5 shows the SSIM values as SNR varies. Each point is averaged over 10 realizations of noise. We see that moving targets are able to be separated even at very low SNRs. For a visual demonstration, we display the reconstruction of the moving targets and stationary components when SNR = 0 dB for a single realization in Figure 6. We see that the reconstructed moving targets are still focused in their correct initial positions.

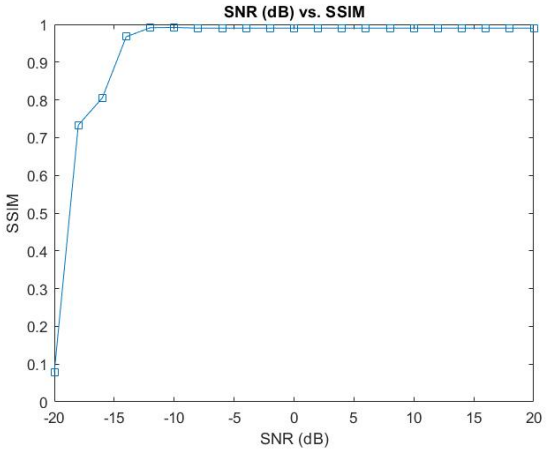

Fig. 5. Signal-to-noise ratio (SNR) vs. structural similarity index (SSIM) of the reconstructed SAR image

V. Conclusion

In this paper, we present a framework based on LRSD for SAR imaging of moving targets. Our method exploits a rank-1 and sparse structure of the underlying unknown reflectivity matrix, reducing computational complexity when compared to typical LRSD frameworks that rely on the nuclear-norm and its associated singular value thresholding. We demonstrate the effectiveness of separating and focusing moving targets

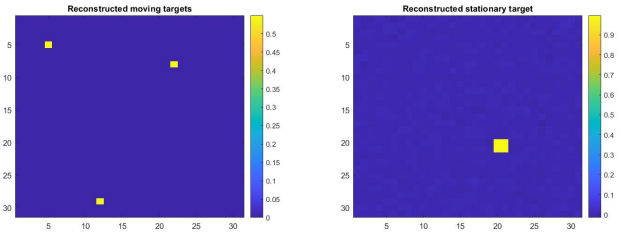

Fig. 6. The reflectivity image reconstructed using the estimated velocities (left) and the reconstruction of the stationary component (right) when SNR = 0dB.

through numerical simulations, and compare the performances of two popular algorithms PGD and ADMM. We see that while ADMM is faster in convergence, both algorithms arrive to the same solution in comparable time. We consider more complex moving target scenes and robustness with respect to clutter in future simulations. We also note that in order to determine the minimum detectable velocity of this approach, a sample complexity analysis on the forward model is needed. Meanwhile, speed of convergence can be addressed through the use of deep learning networks, extensions of this work that are left for future study.

ACKNOWLEDGMENT

This work was supported in part by the Air Force Office of Scientific Research (AFOSR) under the agreement FA9550-19-1-0284, in part by Office of Naval Research (ONR) under the agreement N0001418-1-2068 and in part by the National Science Foundation (NSF) under Grant ECCS-1809234.

REFERENCES

[1] A. Moreira, P. Prats-Iraola, M. Younis, G. Krieger, I. Hajnsek, and K. P. Papathanassiou, "A tutorial on synthetic aperture radar," *IEEE Geoscience and remote sensing magazine*, vol. 1, no. 1, pp. 6–43, 2013.

[2] F. Chen, R. Lasaponara, and N. Masini, "An overview of satellite synthetic aperture radar remote sensing in archaeology: From site detection to monitoring," *Journal of Cultural Heritage*, vol. 23, pp. 5–11, 2017.

[3] E. Ertin, C. D. Austin, S. Sharma, R. L. Moses, and L. C. Potter, "Gotcha experience report: Three-dimensional sar imaging with complete circular apertures," in *Algorithms for synthetic aperture radar imagery XIV*, vol. 6568. International Society for Optics and Photonics, 2007, p. 656802.

[4] L. Wang, C. E. Yarman, and B. Yazici, "Doppler-hitchhiker: A novel passive synthetic aperture radar using ultranarrowband sources of opportunity," *IEEE transactions on geoscience and remote sensing*, vol. 49, no. 10, pp. 3521–3537, 2011.

[5] K. Duman and B. Yazıcı, "Moving target artifacts in bistatic synthetic aperture radar images," *IEEE Transactions on Computational Imaging*, vol. 1, no. 1, pp. 30–43, 2015.

[6] I.-Y. Son and B. Yazici, "Passive polarimetrie multistatic radar for ground moving target," in *2016 IEEE Radar Conference (RadarConf)*. IEEE, 2016, pp. 1–6.

[7] S. Wacks and B. Yazıcı, "Passive synthetic aperture hitchhiker imaging of ground moving targets—part 1: Image formation and velocity estimation," *IEEE transactions on image processing*, vol. 23, no. 6, pp. 2487–2500, 2014.

[8] ——, "Passive synthetic aperture hitchhiker imaging of ground moving targets—part 2: Performance analysis," *IEEE Transactions on Image Processing*, vol. 23, no. 9, pp. 4126–4138, 2014.

[9] L. Wang and B. Yazici, "Bistatic synthetic aperture radar imaging of moving targets using ultra-narrowband continuous waveforms," *SIAM Journal on Imaging Sciences*, vol. 7, no. 2, pp. 824–866, 2014.

[10] S. Wacks and B. Yazıcı, "Bistatic doppler-sar dpca imaging of ground moving targets," in *2014 IEEE Radar Conference*. IEEE, 2014, pp. 1071–1074.

[11] L. Wang and B. Yazici, "Passive imaging of moving targets using sparse distributed apertures," *SIAM Journal on Imaging Sciences*, vol. 5, no. 3, pp. 769–808, 2012.

[12] S. Quegan, "Spotlight synthetic aperture radar: Signal processing algorithms." *JASTP*, vol. 59, pp. 597–598, 1997.

[13] G. Franceschetti and R. Lanari, *Synthetic aperture radar processing*. CRC press, 1999.

[14] C. V. Jakowatz, D. E. Wahl, P. H. Eichel, D. C. Ghiglia, and P. A. Thompson, *Spotlight-Mode Synthetic Aperture Radar: A Signal Processing Approach: A Signal Processing Approach*. Springer Science & Business Media, 2012.

[15] W. Sediono, "Method of measuring doppler shift of moving targets using fmcw maritime radar," in *Proceedings of 2013 IEEE International Conference on Teaching, Assessment and Learning for Engineering (TALE)*, 2013, pp. 378–381.

[16] G. Wang, X.-G. Xia, and V. Chan, "Dual-speed sar imaging of moving targets," *IEEE Transactions on Aerospace and Electronic Systems*, vol. 42, no. 1, pp. 368–379, 2006.

[17] M. I. Skolnik, *Radar handbook*. McGraw-Hill, 2008.

[18] M. I. Pettersson, "Detection of moving targets in wideband sar," *IEEE Transactions on Aerospace and Electronic Systems*, vol. 40, no. 3, pp. 780–796, 2004.

[19] J. H. Ender, "Space-time processing for multichannel synthetic aperture radar," *Electronics & Communication engineering journal*, vol. 11, no. 1, pp. 29–38, 1999.

[20] ——, "Detection and estimation of moving target signals by multi-channel sar," *AEU-ARCHIV FUR ELEKTRONIK UND UBERTRAGUNGSTECHNIK-INTERNATIONAL JOURNAL OF ELECTRONICS AND COMMUNICATIONS*, vol. 50, no. 2, pp. 150–156, 1996.

[21] C. E. Muehe and M. Labitt, "Displaced-phase-center antenna technique," *Lincoln Laboratory Journal*, vol. 12, no. 2, pp. 281–296, 2000.

[22] C. H. Gierull and I. C. Sikaneta, "Raw data based two-aperture sar ground moving target indication," in *IGARSS 2003. 2003 IEEE International Geoscience and Remote Sensing Symposium. Proceedings (IEEE Cat. No. 03CH37477)*, vol. 2. IEEE, 2003, pp. 1032–1034.

[23] A. Budillon, V. Pascazio, and G. Schirinzi, "Amplitude/phase approach for target velocity estimation in at-insar systems," in *2008 IEEE Radar Conference*. IEEE, 2008, pp. 1–5.

[24] C. W. Chen, "Performance assessment of along-track interferometry for detecting ground moving targets," in *Proceedings of the 2004 IEEE Radar Conference (IEEE Cat. No. 04CH37509)*. IEEE, 2004, pp. 99–104.

[25] D. Yang, X. Yang, G. Liao, and S. Zhu, "Strong clutter suppression via rpca in multichannel sar/gmti system," *IEEE geoscience and remote sensing letters*, vol. 12, no. 11, pp. 2237–2241, 2015.

[26] J. Li, Y. Huang, G. Liao, and J. Xu, "Moving target detection via efficient ati-godec approach for multichannel sar system," *IEEE Geoscience and Remote Sensing Letters*, vol. 13, no. 9, pp. 1320–1324, 2016.

[27] C. Schwartz, L. P. Ramos, L. T. Duarte, M. d. S. Pinho, M. I. Pettersson, V. T. Vu, and R. Machado, "Change detection in uwb sar images based on robust principal component analysis," *Remote Sensing*, vol. 12, no. 12, p. 1916, 2020.

[28] G. Xu, X. Wang, Y. Huang, L. Cai, and Z. Jiang, "Joint multi-channel sparse method of robust pca for sar ground moving target image indication," in *IGARSS 2019-2019 IEEE International Geoscience and Remote Sensing Symposium*. IEEE, 2019, pp. 1709–1712.

[29] X. Jia and H. Song, "Clutter suppression for multichannel wide area surveillance system via a combination of stap and rpca," in *2019 6th Asia-Pacific Conference on Synthetic Aperture Radar (APSAR)*. IEEE, 2019, pp. 1–4.

[30] H. Yan, R. Wang, F. Li, Y. Deng, and Y. Liu, "Ground moving target extraction in a multichannel wide-area surveillance SAR/GMTI system via the relaxed PCP," *IEEE Geoscience and Remote Sensing Letters*, vol. 10, no. 3, pp. 617–621, 2013.

[31] J. Ender, "Multi-Channel GMTI via Approximated Observation."

[32] M. Yasin, M. Cetin, and A. S. Khwaja, "SAR imaging of moving targets by subaperture based low-rank and sparse decomposition," in *2017 25th Signal Processing and Communications Applications Conference, SIU 2017*, 2017.

[33] P. Huang, J. Ma, H. Xu, X. Liu, X. Jiang, and G. Liao, "Moving Target Focusing in SAR Imagery Based on Subaperture Processing and DART," *IEEE Geoscience and Remote Sensing Letters*, pp. 1–5, 2020.
[34] M. Çetin, M. Yasin, and A. S. Khwaja, "A subaperture based approach for SAR moving target imaging by low-rank and sparse decomposition," no. April 2018, p. 19, 2018.
[35] F. Biondi, "Low rank plus sparse decomposition of synthetic aperture radar data for maritime surveillance," *2016 4th International Workshop on Compressed Sensing Theory and its Applications to Radar, Sonar and Remote Sensing, CoSeRa 2016*, vol. 6, no. 2, pp. 75–79, 2016.
[36] K. Duman and B. Yazici, "Ground moving target imaging using bistatic synthetic aperture radar," in *2013 IEEE Radar Conference (RadarCon13)*. IEEE, 2013, pp. 1–4.
[37] L. Wang and B. Yazici, "Passive imaging of moving targets exploiting multiple scattering using sparse distributed apertures," *Inverse Problems*, vol. 28, no. 12, p. 125009, 2012.
[38] ——, "Ground moving target imaging using ultranarrowband continuous wave synthetic aperture radar," *IEEE transactions on geoscience and remote sensing*, vol. 51, no. 9, pp. 4893–4910, 2013.
[39] C. Guyon, T. Bouwmans, and E.-H. Zahzah, "Foreground detection via robust low rank matrix factorization including spatial constraint with iterative reweighted regression," in *Proceedings of the 21st International Conference on Pattern Recognition (ICPR2012)*. IEEE, 2012, pp. 2805–2808.
[40] ——, "Moving object detection via robust low rank matrix decomposition with irls scheme," in *International symposium on visual computing*. Springer, 2012, pp. 665–674.
[41] A. Beck and M. Teboulle, "Fast gradient-based algorithms for constrained total variation image denoising and deblurring problems," *IEEE transactions on image processing*, vol. 18, no. 11, pp. 2419–2434, 2009.
[42] C. H. Casteel Jr, L. A. Gorham, M. J. Minardi, S. M. Scarborough, K. D. Naidu, and U. K. Majumder, "A challenge problem for 2d/3d imaging of targets from a volumetric data set in an urban environment," in *Algorithms for Synthetic Aperture Radar Imagery XIV*, vol. 6568. International Society for Optics and Photonics, 2007, p. 65680D.